Research Article | Vol. 27, No. 14 | 8 Jul 2019 | OPTICS EXPRESS 19463
Optics EXPRESS

Extremely anisotropic epsilon-near-zero media in waveguide metamaterials

WENJIE JI,[1] JIE LUO,[1,2,4] AND YUN LAI[2,3]

[1]School of Physical Science and Technology, Soochow University, Suzhou 215006, China
[2]National Laboratory of Solid State Microstructures, School of Physics, and Collaborative Innovation Center of Advanced Microstructures, Nanjing University, Nanjing 210093, China
[3]laiyun@nju.edu.cn
[4]luojie@suda.edu.cn

Abstract: Extremely anisotropic media such as anisotropic zero-index media allow wave propagation in extraordinary ways that are absent in isotropic systems. Here, we propose an approach to realize a type of extremely anisotropic effective epsilon-near-zero media by exploiting anisotropic waveguide metamaterials. The metamaterial is composed of two kinds of dielectrics with metal wires in waveguides. Extreme anisotropy is realized by alternating layers of the two kinds of dielectrics, which lead to different cut-off frequencies for transverse electric modes in different directions. Anisotropic effective epsilon-near-zero media with low loss can be obtained around the cutoff frequencies. Based on the extreme anisotropy, the unique phenomena of directive emission, nearly perfect bending waveguides and arbitrary control of energy flux are demonstrated. Interestingly, subwavelength focusing of energy flux with a spotsize $< 0.2\lambda$ is observed (λ is the wavelength in free space). Our work provides a convenient approach for the realization of extremely anisotropic epsilon-near-zero media and unique applications in low-loss waveguide metamaterials.

1. Introduction

Electromagnetic media with extremely anisotropic parameters and electromagnetic responses, such as hyperbolic media [1–4] and anisotropic zero-index media (ZIM) [5–29], have generated important and rich physics, as well as wide applications in recent years. For example, anisotropic ZIM possess near-zero permittivity/permeability in one direction and finite permittivity/permeability in the other directions. This leads to almost flat equal frequency contours (EFCs), enabling many interesting applications, such as arbitrary flux control [7,8], perfect exotic waveguides [9–12], directive emission [13–15], power combination [16,17], perfect electromagnetic absorption [18–22], strong Purcell effect [24], etc. Most of them are absent in isotropic ZIM.

The realization of anisotropic epsilon-near-zero (ENZ) media usually require metallic components with negative-ε response [30–33] at optical frequencies. This structure, however, suffer from dissipative losses. At lower frequencies such as terahertz and microwave frequencies, metals behave as perfect electric conductors (PECs), which do not support the negative-ε response. One way to achieve negative-ε response at low frequencies is to construct artificial media with metal wires. However, spatial dispersions and mode coupling effects become inevitable [34]. Very recently, another novel route to realize effective negative-ε media with low loss has been proposed by exploiting isotropic waveguide metamaterials (WMMs), which are composed of bounded PEC waveguides filled with positive-ε media (i.e. dielectrics) only [35,36]. Structural dispersion of waveguide modes leads to effective negative-ε response, which inspired a variety of theoretical and experimental investigation of plasmonic phenomena [37–40]. However, we notice that all the proposed WMMs in the previous works are effectively isotropic materials. Thus, one interesting question arises: is it also possible to realize low-loss extremely anisotropic media with unique features and applications by WMMs?

#366190 https://doi.org/10.1364/OE.27.019463
Journal © 2019 Received 26 Apr 2019; revised 9 Jun 2019; accepted 17 Jun 2019; published 26 Jun 2019

Optics EXPRESS

In this work, we demonstrate that lossless extremely anisotropic WMMs can indeed be realized by using parallel-plate waveguides (PPWs) or rectangular waveguides filled with alternating layers of two kinds of dielectrics and metal wires. By adjusting the thicknesses of the two kinds of dielectrics, we can obtain different effective permittivities in different directions. Interestingly, effective anisotropic ENZ media with low loss can be achieved round the cutoff frequency of transverse electric (TE) modes. As the consequences of extreme anisotropy, we demonstrate the unique phenomena of directive emission, nearly perfect exotic waveguides and arbitrary control of energy flux, which are all based on the proposed effective anisotropic ENZ media. Moreover, subwavelength focusing of energy flux with a spotsize $<0.2\lambda$ (λ is the wavelength in free space), as the unique feature of the anisotropic ENZ media, is also observed.

2. Anisotropic waveguide metamaterials

For the in-plane anisotropic medium characterized by a relative permittivity tensor with orthogonal principle axes $\begin{pmatrix} \varepsilon_{x,eff} & \\ & \varepsilon_{y,eff} \end{pmatrix}$ (Fig. 1(a)), the dispersion relation or EFC for electromagnetic waves with magnetic fields oriented in the z direction is determined by the following equation,

$$\frac{k_x^2}{\varepsilon_{y,eff}} + \frac{k_y^2}{\varepsilon_{x,eff}} = k_0^2, \tag{1}$$

where k_x and k_y are the propagation vectors in the x and y directions, respectively. $k_0 = 2\pi f/c$ is the wave number in free space. f and c are the frequency and light velocity in free space, respectively.

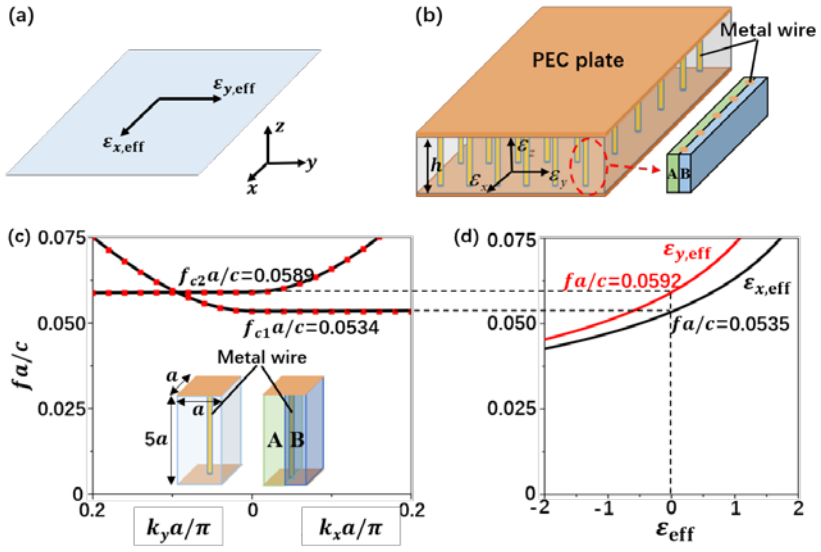

Fig. 1. Illustrations of (a) a two-dimensional effective anisotropic medium, (b) an anisotropic WMM composed of a metal-wire-added PPW and two kinds of filling dielectrics A and B. (c) Band structures of the anisotropic WMM when the filling material is a uniform anisotropic dielectric (black lines) or a dielectric multilayer (red dots). The corresponding unit cells of the WMM are illustrated by the insets. (d) Effective permittivities of the anisotropic WMM obtained from Eq. (2).

Optics EXPRESS

For the anisotropic ENZ media with $\varepsilon_{y,eff} >> \left|\varepsilon_{x,eff}\right| \approx 0$ or $\varepsilon_{x,eff} >> \left|\varepsilon_{y,eff}\right| \approx 0$, the EFC becomes almost flat lines. To realize such anisotropic ENZ media, we propose an anisotropic WMM consisting of a PEC PPW filled with an in-plane anisotropic dielectric medium, as sketched in Fig. 1(b). Such an anisotropic dielectric medium possesses a relative permittivity tensor $\begin{pmatrix} \varepsilon_x & & \\ & \varepsilon_y & \\ & & \varepsilon_z \end{pmatrix}$ with $\varepsilon_x \neq \varepsilon_y$. In this case, the waveguide modes with electric fields polarized in the x and y directions exhibit different electromagnetic responses. We notice that such an anisotropic medium with $\varepsilon_x = \varepsilon_z \neq \varepsilon_y$ can be easily realized by using a dielectric multilayer structure. Here, we alternately stack dielectrics A and B along the y direction in deep-subwavelength scale (see the inset in Fig. 1(b)) to achieve $\left(\varepsilon_A d_A + \varepsilon_B d_B\right) / \left(d_A + d_B\right) = \varepsilon_x = \varepsilon_z$ and $\varepsilon_A \varepsilon_B \left(d_A + d_B\right) / \left(\varepsilon_B d_A + \varepsilon_A d_B\right) = \varepsilon_y$ [41], where ε_A (ε_B) and d_A (d_B) denote the relative permittivity and thickness of dielectric A (B), respectively.

Normally, a PPW supports a variety number of waveguide modes. In order to guarantee that the anisotropic medium-filled PPW can be regarded as a uniform anisotropic WMM, single-mode condition should be satisfied, i.e., there is only one dominant mode in the PPW [42,43]. Otherwise, the homogenized WMM don't have single-valued effective parameters, because different modes possess different structural dispersions. Moreover, in order to endow the homogenized WMM with the dispersion of Eq. (1), the fundamental TE mode (with electric fields polarized in the xy plane) should be the dominant mode inside the PPW.

Actually, the anisotropic medium-filled PPW generally does not support pure TE modes [44–46]. Interestingly, inspired by previous works [35–37], we find that waveguide modes can be stirred by using metal wires to connect the PEC plates of the PPW. To investigate the effects of the metal wires, we study band structures and eigenmodes of the anisotropic medium-filled PPW in the existence of metal wires by using software COMSOL Multiphysics. The black lines in Fig. 1(c) show the band structures of the PPW filled with a uniform anisotropic medium with $\varepsilon_x = 3.5$ and $\varepsilon_y = 2.86$. The lengths of the PPW unit cell are set as a, a and ($h = 5a$) in the x, y and z directions, respectively, as illustrated by the left inset in Fig. 1(c). A vertical oriented metal wire (radius $0.1a$) connecting PEC plates is placed in the center. For comparison, we also use conventional isotropic dielectrics A and B to realize the anisotropic medium (see the right inset in Fig. 1(c)). The relevant parameters are $\varepsilon_A = 5$, $\varepsilon_B = 2$ and $d_A = d_B = 0.5a$. It is seen from Fig. 1(c) that the corresponding band structures (red dots) coincide well with those related to the case with a uniform anisotropic medium (black lines).

Owing to the existence of the in-plane anisotropic medium inside the PPW, the band structures show strong anisotropy along the k_x and k_y directions. Actually, both the first two bands displayed in Fig. 1(c) correspond to the TE_1 mode with E_x and E_y having a near π phase difference between two PEC plates. They originate from the split TE_1 mode due to the in-plane anisotropy. Flat bands along the k_x (k_y) direction in the first (second) band are related to the longitudinal modes that cannot be excited directly [47,48]. Consequently, for frequencies above the cutoff frequency of TE_1 mode (i.e. the bottom of the first band) and below the cutoff frequency of TE_2 mode (i.e. the bottom of the third band, not shown here), the single-mode condition is satisfied. In this case, such a PPW model can be regarded as a homogenous anisotropic WMM.

Optics EXPRESS

Interestingly, around the cutoff frequency of the first band $f_{c1}a/c = 0.0534$, we have $k_y \approx 0$ (i.e., the propagation constant in the y direction is near zero), indicating that the WMM possesses a near-zero $\varepsilon_{x,eff}$. On the other hand, at the cutoff frequency of the second band $f_{c2}a/c = 0.0589$, we obtain $k_x \approx 0$ and a near-zero $\varepsilon_{y,eff}$ of the WMM. Thereby, we see that such a WMM can work as an effective anisotropic ENZ medium around the cutoff frequencies of the first two bands.

For further verification, we approximately derive structural-dispersion-induced effective permittivity of the anisotropic WMM in a similar way of the isotropic case [35] as,

$$\varepsilon_{x,eff} = \varepsilon_x - c^2/4f^2h^2 \text{ and } \varepsilon_{y,eff} = \varepsilon_y - c^2/4f^2h^2. \quad (2)$$

In Fig. 1(d), we plot the effective parameters according to Eq. (2), showing $\varepsilon_{x,eff} = 0$ at the frequency $fa/c = a/2h\sqrt{\varepsilon_x} \approx 0.0535$ and $\varepsilon_{y,eff} = 0$ at the frequency $fa/c = a/2h\sqrt{\varepsilon_y} \approx 0.0592$. These frequencies coincide well with the cutoff frequencies of the first two bands in Fig. 1(c). This further confirms that the WMM can be homogenized as effective anisotropic ZIM nearby the cutoff frequencies.

Here we note that the dielectrics A and B with $\varepsilon_A = 5$ and $\varepsilon_B = 2$ can be easily realized at microwave frequencies by plastic materials such as FR-4 and PTFE. Actually, almost arbitrary dielectric materials with a relatively large refractive index contrast can be utilized to realize the effective anisotropic ZIM. By controlling the waveguide size h, the effective parameter $\varepsilon_{x,eff}$ or $\varepsilon_{y,eff}$ can be tuned to be zero at the desired operating frequency, as indicated in Eq. (2).

3. Phenomena induced by anisotropic ENZ media

It is worth noting that the effective anisotropic ENZ media based on WMMs exhibit very little loss at low frequencies (e.g., terahertz and microwave frequencies). Therefore, the proposed anisotropic ENZ media are suitable for various applications that require low loss, such as high transmission in exotic waveguides [9–12]. Moreover, we find that the homogenization of such effective anisotropic ENZ media is valid even in the deep-subwavelength scale, which is of great advantage for sub-wavelength applications like the arbitrary control of energy flux [7,8]. In the following, we numerically show that such anisotropic ENZ media based on the WMMs can provide an excellent platform for realizing some ZIM phenomena and applications, including directive emission, nearly perfect exotic waveguides and subwavelength focusing of energy flux.

In the first example, we demonstrate the phenomenon of direction emission. We embed a magnetic-current line source oriented in the z direction in the center of the anisotropic WMM designed above, which is surrounded by an isotropic WMM with a filling dielectric medium of $\varepsilon_r = 4$ (see the inset in Fig. 2(b)). The working frequency is chosen as $fa/c = 0.0590$, a bit above the cutoff frequency of the second band. To study emitted waves of the line source, we plot EFCs of the WMMs at the working frequency in Fig. 2(a). The red and gray lines denote the EFCs of the anisotropic and isotropic WMMs, showing a flat ellipse and a circle, respectively. The flat elliptical EFC indicates that the anisotropic WMM behaves as an effective anisotropic ENZ medium with $\varepsilon_{x,eff} >> \varepsilon_{y,eff} \approx 0^+$. In Fig. 2(b), we construct the propagation directions of emitted waves from the EFCs and conservation of wave-vector component parallel to the anisotropic/isotropic WMM surface. It is seen that emitted waves in the left and right sides are concentrated around the normal of the surface, indicating quite good directivity of the emitted waves. For demonstrations, we perform numerical simulations based on software COMSOL Multiphysics. Figure 2(c) shows the distribution of H_z (i.e. the z-component of magnetic fields) in the middle plane of the waveguide. Apparently, good plane wavefronts of

Optics EXPRESS

emitted waves and good directional radiation performance in the left and right sides can be observed. Furthermore, we re-simulate the performance of emission in a two-dimensional effective model in Fig. 2(d), in which the anisotropic ENZ medium (or the background isotropic medium) is characterized by $\varepsilon_{x,eff} \approx 0.7$ and $\varepsilon_{y,eff} \approx 0.035$ (or $\varepsilon_{eff} \approx 1.1$). A monopolar point source with magnetic fields polarized in the z direction is embedded in the center of the anisotropic ENZ medium. We can see that the H_z-distribution in Fig. 2(d) is almost the same as that in Fig. 2(c), thus confirming the good directional radiation performance within the effective anisotropic ENZ medium by using anisotropic WMMs.

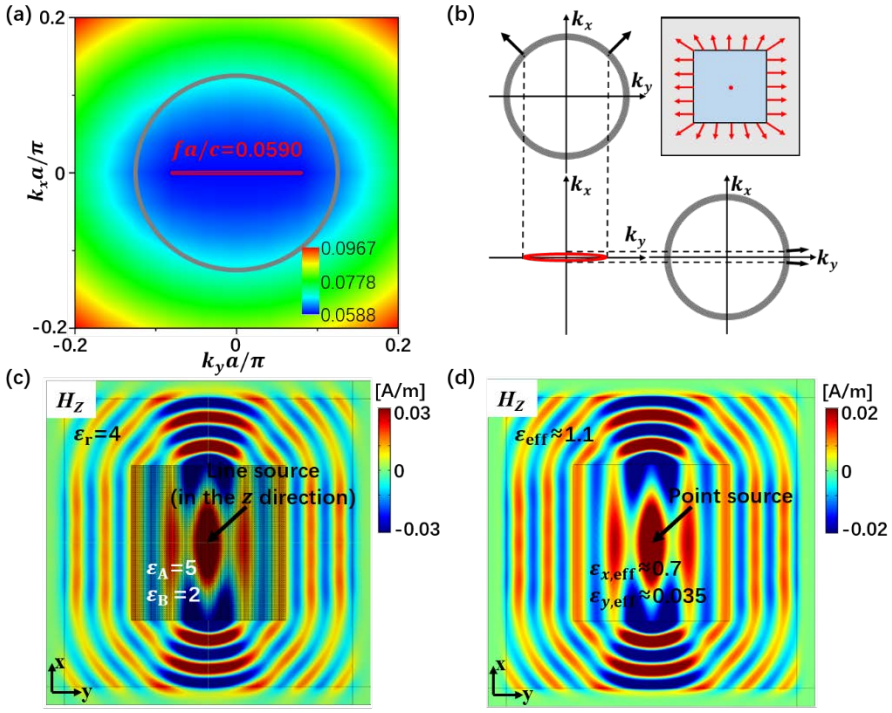

Fig. 2. (a) EFCs of the designed anisotropic WMM (red lines) and background isotropic WMM (gray lines) at the working frequency $fa/c = 0.0590$. (b) Schematic graph of the radiated waves obtained from EFCs based on conservation of surface-parallel wave vector. A source is placed in center of the anisotropic ENZ medium in the background of an isotropic medium. (c) The H_z-distribution in the middle plane of the waveguide for the actual WMM model. A magnetic-current line source oriented in the z direction is placed in the center of the anisotropic WMM. (d) The H_z-distribution in the two-dimensional effective medium model. A monopolar point source is placed in the center of the effective anisotropic ENZ medium.

Moreover, we consider the working frequency $fa/c = 0.0587$, a bit below the cutoff frequency of the second band. In this case, there is no solution for k_x if k_y is small. Thus, the EFC turns to be a flat hyperbola (red lines in Fig. 3(a)), meaning that the WMM works as an effective hyperbolic ENZ medium with $\varepsilon_{x,eff} >> \left|\varepsilon_{y,eff}\right|$ and $\varepsilon_{y,eff} \approx 0^-$ [25,26]. Although the EFC turns to be hyperbolic, it is still quite flat compared with the EFC of the background isotropic WMM (gray lines in Fig. 3(a)). Therefore, emitted waves in the left and right sides will still be concentrated around the normal of the surface, as illustrated in Fig. 3(b). The simulated H_z-distributions in the actual WMM model (Fig. 3(c)) and the two-dimensional

Optics EXPRESS

effective medium model (Fig. 3(d)) both confirm the good directivity of emitted waves in the left and right sides. Here, the parameters of the hyperbolic ENZ medium in the effective medium model in Fig. 3(d) are $\varepsilon_{x,eff} \approx 0.65$ and $\varepsilon_{y,eff} \approx (-1+0.1i)\times 10^{-3}$. A little loss is introduced to $\varepsilon_{y,eff}$ to avoid the influence of infinitely large wave vectors in the effective hyperbolic ENZ medium.

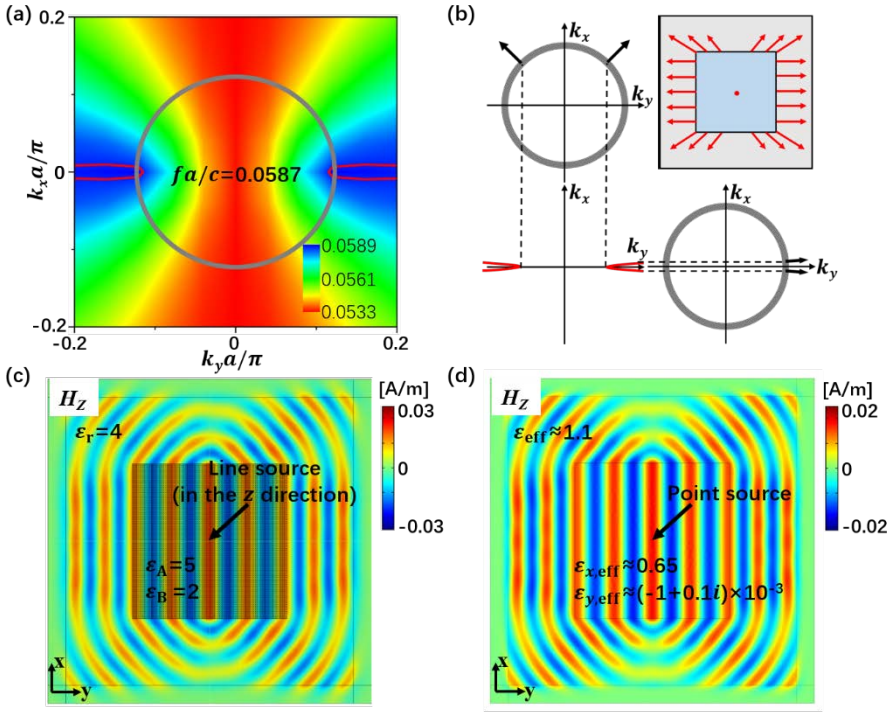

Fig. 3. (a) EFCs of the designed anisotropic WMM (red lines) and background isotropic WMM (gray lines) at the operating frequency $fa/c = 0.0587$. (b) Schematic graph of the radiated waves obtained from EFCs based on conservation of surface-parallel wave vector. A source is placed in the center of the anisotropic ENZ medium in the background of an isotropic medium. (c) The H_z-distribution in the middle plane of the waveguide for the actual WMM model. A magnetic-current line source oriented in the z direction is placed in the center of the anisotropic WMM. (d) The H_z-distribution in the two-dimensional effective medium model. A monopolar point source is placed in the center of the effective anisotropic ENZ medium.

In the second example, we demonstrate that the effective anisotropic ENZ medium is capable of realizing nearly perfect wave transmission in exotic waveguides, which is robust to the irregular waveguide walls and bending angles. In Fig. 4(a), we take a wavy bent rectangular waveguide as an example. The cross section with dimensions of $10a$ in the x direction and $5a$ in the z direction is illustrated by the inset in Fig. 4(a). A TE_{01} mode as the dominant mode is excited on the left input port. In this case, the effective parameters in Eq. (2) are still valid for the rectangular waveguide [36]. Thus, the input and output regions filled with a dielectric medium with $\varepsilon_r = 3.5$ serve as isotropic WMMs with $\varepsilon_{eff} \approx 0.63$ at the working frequency $fa/c = 0.0590$. While the wavy region filled with periodic layers of dielectrics A and B and metal wires works as an anisotropic ENZ medium with $\varepsilon_{x,eff} >> \varepsilon_{y,eff} \approx 0^+$, which is the same as that in Fig. 2. From the distribution of H_z in the middle plane of the waveguide, we can

Optics EXPRESS

clearly observe almost perfect transmission (transmittance>0.97) and good plane wavefronts of waves through such a wavy waveguide. For comparison, in Fig. 4(b), we replace the anisotropic WMM in the wavy region by an isotropic WMM (the same as that in the input region). The H_z -distribution clearly show the low transmission (transmittance~0.53) and great distortions in wavefronts caused by the wavy waveguide walls.

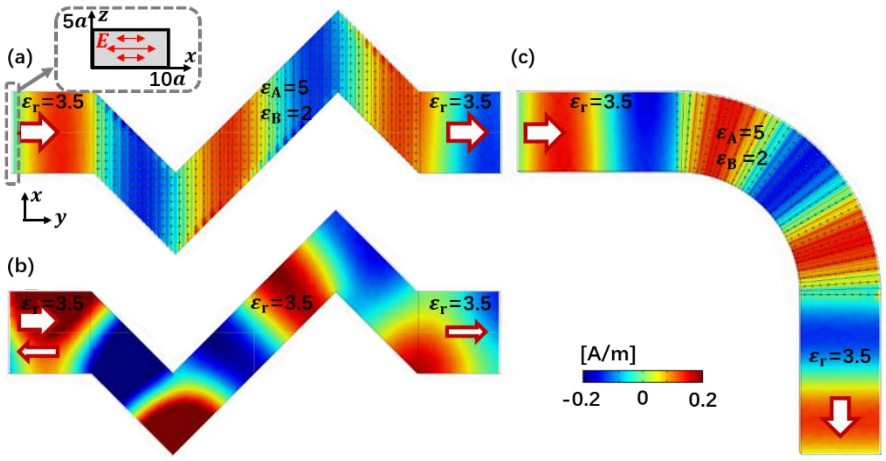

Fig. 4. The distribution of H_z in the middle part of several rectangular waveguides. (a) A wavy waveguide embedded with an anisotropic WMM with $\varepsilon_{x,eff} >> \varepsilon_{y,eff} \approx 0^+$. (b) A wavy waveguide embedded with an isotropic WMM with $\varepsilon_{eff} \approx 0.63$. (c) A 90° waveguide bend, whose bending region is embedded with an anisotropic WMM with a near-zero effective permittivity along the propagation direction. The cross section of the rectangular waveguides is illustrated by the inset in (a). A TE_{01} mode with working frequency of $fa/c = 0.0590$ is excited on the left port.

Moreover, we show the performance of the effective anisotropic ENZ medium in a 90° waveguide bend, as shown in Fig. 4(c). The waveguide here is the same as that in Fig. 4(a), but the walls are bent at 90°. In this situation, the anisotropic WMM in the bending region serves as an effective anisotropic ENZ medium with a near-zero effective permittivity along the propagation direction. Figure 4(c) presents the H_z -distribution under the excitation of TE_{01} mode, showing almost perfect transmission (transmittance>0.98) and good plane wavefronts of waves in such a 90° waveguide bend.

We note that the high transmission is robust to the irregular waveguide walls and bending angles. The underlying physics can be explained based on transformation optics. It is found that an arbitrarily shaped waveguide filled the anisotropic ENZ medium in physical space is equivalent to a straight waveguide filled with an inhomogeneous anisotropic ENZ medium in the virtual space [9,10,49]. And in the inhomogeneous anisotropic ENZ medium, robust high transmission can be usually obtained attributing to energy flux redistribution and averaging effect of parameters, as we shall demonstrate in the third example.

In the third example, we demonstrate that robust high transmission and interesting applications like subwavelength focusing of energy flux can be achieved in an inhomogeneous anisotropic ENZ medium with $\varepsilon_{y,eff} \approx 0$ and $\varepsilon_{x,eff} = f(x,y) >> \left|\varepsilon_{y,eff}\right|$, where $f(x,y)$ is an inhomogeneity profile. In such a system, the energy flux is concentrated to low-$\varepsilon_{x,eff}$ region even in the subwavelength scale when waves propagate along the y direction. This is accomplished by evanescent waves that can efficiently transfer energy flux in the perpendicular

Optics EXPRESS

direction of propagation and redistribute the energy flux in such an inhomogeneous system [7,49].

Figure 5(a) shows a schematic graph of the proposed model. It is a rectangular waveguide with cross-section dimensions of $15a$ and $5a$ in the x and z directions, respectively. A TE_{01} mode at working frequency $fa/c = 0.0671$ is excited on the left input port. In this case, the input and output regions filled with a dielectric medium ($\varepsilon_r = 5.63$) work as isotropic WMMs with $\varepsilon_{eff} \approx 3.4$. The middle region (light blue region) is filled with a periodic multilayer composed of two kinds of dielectrics A' and B' ($\varepsilon_{A'} = 1.25$, $\varepsilon_{B'} = 10$ and $d_{A'} = d_{B'} = 0.5a$) and metal wires (radius $0.1a$), serving as an effective anisotropic ENZ medium with $\varepsilon_{x,eff} \approx 3.4$ and $\varepsilon_{y,eff} \approx 0.001$, as shown by the upper inset in Fig. 5(a). The central part (light green region) is also filled with periodic metal wires (radius $0.01a$) and a periodic multilayer, but the composite dielectrics are different. Here, dielectrics A'' and B'' with $\varepsilon_{A''} = 2$, $\varepsilon_{B''} = 2.5$ and $d_{A''} = d_{B''} = 0.075a$ are utilized, so that the center part works as an effective anisotropic ENZ medium with $\varepsilon_{x,eff} \approx 0.029$ and $\varepsilon_{y,eff} \approx 0.001$. Thus, an inhomogeneous anisotropic ENZ system is constructed with low- $\varepsilon_{x,eff}$ region in the center.

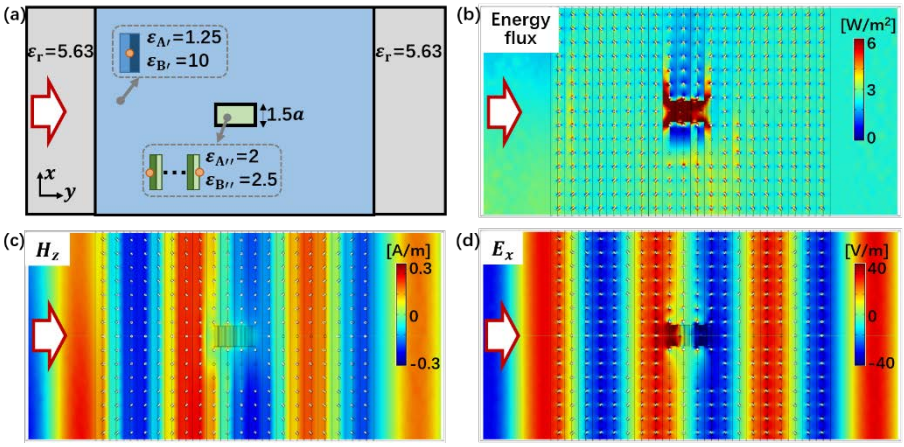

Fig. 5. (a) Schematic graph of a model for subwavelength focusing of electromagnetic energy flux, which is composed of an anisotropic WMM with $\varepsilon_{x,eff} \approx 3.4$ and $\varepsilon_{y,eff} \approx 0.001$ (light blue region), an anisotropic WMM with $\varepsilon_{x,eff} \approx 0.029$ and $\varepsilon_{y,eff} \approx 0.001$ (light green region), and an isotropic WMM with $\varepsilon_{eff} \approx 3.4$ as the background medium (gray region). The unit cells and relevant parameters are shown in the inset graphs. The waveguide is a rectangular waveguide with cross-section dimensions $15a$ and $5a$ in the x and z directions, respectively. Snapshots of (b) total energy flux density, (c) H_z , (d) E_x when a TE_{01} mode with operating frequency of $fa/c = 0.0671$ is excited on the left port.

Then, we simulate total energy flux distribution in Fig. 5(b), showing the robust high transmission (transmittance>0.91) and energy flux concentration in the central low- $\varepsilon_{x,eff}$ region. It is interesting to point out that the width of the central part is only $1.5a$ (i.e., 0.18λ with λ being the wavelength in the background isotropic WMM) in the x direction, demonstrating the subwavelength focusing of energy flux. Actually, the width of the central part can be further reduced to obtain sharper focused flux spot. For further study, the distributions of H_z and E_x are also simulated, as shown in Figs. 5(c) and 5(d), respectively.

Optics EXPRESS

We can see that the uniformity of H_z in the x direction is not largely disturbed by the inhomogeneity due to the near-zero $\varepsilon_{y,eff}$. On the other hand, the distribution of E_x is mainly determined by the continuity condition of the x-component of electric displacement. Due to the low-$\varepsilon_{x,eff}$ in the central part, E_x is greatly enhanced, as shown in Fig. 5(d). Therefore, we obtain focusing of energy flux in the central low-$\varepsilon_{x,eff}$ region.

4. Conclusions

To conclude, we have proposed a design method for low-loss extremely anisotropic WMMs by exploiting metal-wire-added waveguides embedded with two kinds of dielectrics. The two kinds of dielectrics are periodically stacked in one direction to obtain in-plane anisotropic structural dispersions. Through the energy band analysis, it is found that effective anisotropic ZIM can be obtained at the cutoff frequencies of the first two bands. Owing to the advantages of low loss and simple design, directive emission, nearly perfect exotic waveguides and subwavelength focusing of energy flux are demonstrated. This methodology can also be expected to realize other extremely anisotropic media like hyperbolic media, which may have capabilities for designing advanced electromagnetic devices at both microwave and terahertz frequencies.

Funding

National Key R&D Program of China (2017YFA0303702), National Natural Science Foundation of China (61671314, 11574226, 11634005, 11704271), Natural Science Foundation of Jiangsu Province (BK20170326), Natural Science Foundation for Colleges and Universities in Jiangsu Province of China (17KJB140019), the Priority Academic Program Development (PAPD) of Jiangsu Higher Education Institutions.

References

1. D. R. Smith and D. Schurig, “Electromagnetic wave propagation in media with indefinite permittivity and permeability tensors,” Phys. Rev. Lett. **90**(7), 077405 (2003).
2. A. Poddubny, I. Iorsh, P. Belov, and Y. Kivshar, “Hyperbolic metamaterials,” Nat. Photonics **7**(12), 948–957 (2013).
3. W. Ma, P. Alonso-González, S. Li, A. Y. Nikitin, J. Yuan, J. Martín-Sánchez, J. Taboada-Gutiérrez, I. Amenabar, P. Li, S. Vélez, C. Tollan, Z. Dai, Y. Zhang, S. Sriram, K. Kalantar-Zadeh, S. T. Lee, R. Hillenbrand, and Q. Bao, “In-plane anisotropic and ultra-low-loss polaritons in a natural van der Waals crystal,” Nature **562**(7728), 557–562 (2018).
4. P. Li, I. Dolado, F. J. Alfaro-Mozaz, F. Casanova, L. E. Hueso, S. Liu, J. H. Edgar, A. Y. Nikitin, S. Vélez, and R. Hillenbrand, “Infrared hyperbolic metasurface based on nanostructured van der Waals materials,” Science **359**(6378), 892–896 (2018).
5. M. G. Silveirinha and N. Engheta, “Transporting an image through a subwavelength hole,” Phys. Rev. Lett. **102**(10), 103902 (2009).
6. M. Memarian and G. V. Eleftheriades, “Light concentration using hetero-junctions of anisotropic low permittivity metamaterials,” Light Sci. Appl. **2**(11), e114 (2013).
7. J. Luo, W. Lu, Z. Hang, H. Chen, B. Hou, Y. Lai, and C. T. Chan, “Arbitrary control of electromagnetic flux in inhomogeneous anisotropic media with near-zero index,” Phys. Rev. Lett. **112**(7), 073903 (2014).
8. Y. Li, H. T. Jiang, W. W. Liu, J. Ran, Y. Lai, and H. Chen, “Experimental realization of subwavelength flux manipulation in anisotropic near-zero index metamaterials,” EPL **113**(5), 57006 (2016).
9. J. Luo, P. Xu, H. Chen, B. Hou, L. Gao, and Y. Lai, “Realizing almost perfect bending waveguides with anisotropic epsilon-near-zero metamaterials,” Appl. Phys. Lett. **100**(22), 221903 (2012).
10. J. Luo and Y. Lai, “Anisotropic zero-index waveguide with arbitrary shapes,” Sci. Rep. **4**(1), 5875 (2014).
11. H. F. Ma, J. H. Shi, W. X. Jiang, and T. J. Cui, “Experimental realization of bending waveguide using anisotropic zero-index materials,” Appl. Phys. Lett. **101**(25), 253513 (2012).
12. H. F. Ma, J. H. Shi, Q. Cheng, and T. J. Cui, “Experimental verification of supercoupling and cloaking using mu-near-zero materials based on a waveguide,” Appl. Phys. Lett. **103**(2), 021908 (2013).
13. S. Enoch, G. Tayeb, P. Sabouroux, N. Guérin, and P. Vincent, “A metamaterial for directive emission,” Phys. Rev. Lett. **89**(21), 213902 (2002).
14. J. Luo, P. Xu, and L. Gao, “Directive emission based on one-dimensional metal heterostructures,” J. Opt. Soc. Am. B **29**(1), 35–39 (2012).

Optics EXPRESS

15. Y. Yuan, L. Shen, L. Ran, T. Jiang, J. Huangfu, and J. Kong, "Directive emission based on anisotropic metamaterials," Phys. Rev. A **77**(5), 053821 (2008).
16. Q. Cheng, W. X. Jiang, and T. J. Cui, "Spatial power combination for omnidirectional radiation via anisotropic metamaterials," Phys. Rev. Lett. **108**(21), 213903 (2012).
17. Q. Cheng, B. Geng Cai, W. Xiang Jiang, H. Feng Ma, and T. Jun Cui, "Spatial power combination within fan-shaped region using anisotropic zero-index metamaterials," Appl. Phys. Lett. **101**(14), 141902 (2012).
18. J. Luo, S. Li, B. Hou, and Y. Lai, "Unified theory for perfect absorption in ultrathin absorptive films with constant tangential electric or magnetic fields," Phys. Rev. B Condens. Matter Mater. Phys. **90**(16), 165128 (2014).
19. S. Feng and K. Halterman, "Coherent perfect absorption in epsilon-near-zero metamaterials," Phys. Rev. B Condens. Matter Mater. Phys. **86**(16), 165103 (2012).
20. J. Rensberg, Y. Zhou, S. Richter, C. Wan, S. Zhang, P. Schöppe, R. Schmidt-Grund, S. Ramanathan, F. Capasso, M. A. Kats, and C. Ronning, "Epsilon-near-zero substrate engineering for ultrathin-film perfect absorbers," Phys. Rev. Appl. **8**(1), 014009 (2017).
21. S. Zhong, Y. Ma, and S. He, "Perfect absorption in ultrathin anisotropic ϵ-near-zero metamaterials," Appl. Phys. Lett. **105**(2), 023504 (2014).
22. H. Jiang, W. Liu, K. Yu, K. Fang, Y. Sun, Y. Li, and H. Chen, "Experimental verification of loss-induced field enhancement and collimation in anisotropic μ-near-zero metamaterials," Phys. Rev. B Condens. Matter Mater. Phys. **91**(4), 045302 (2015).
23. I. Liberal and N. Engheta, "Near-zero refractive index photonics," Nat. Photonics **11**(3), 149–158 (2017).
24. A. V. Chebykin, A. A. Orlov, A. S. Shalin, A. N. Poddubny, and P. A. Belov, "Strong Purcell effect in anisotropic ϵ-near-zero metamaterials," Phys. Rev. B Condens. Matter Mater. Phys. **91**(20), 205126 (2015).
25. J. Luo, Y. Xu, H. Chen, B. Hou, W. Lu, and Y. Lai, "Oblique total transmissions through epsilon-near-zero metamaterials with hyperbolic dispersions," EPL **101**(4), 44001 (2013).
26. X. Chen, C. Zhang, F. Yang, G. Liang, Q. Li, and L. J. Guo, "Plasmonic lithography utilizing epsilon near zero hyperbolic metamaterial," ACS Nano **11**(10), 9863–9868 (2017).
27. J. Luo, J. Li, and Y. Lai, "Electromagnetic impurity-immunity induced by parity-time symmetry," Phys. Rev. X **8**(3), 031035 (2018).
28. X. Zhang and Y. Wu, "Effective medium theory for anisotropic metamaterials," Sci. Rep. **5**(1), 7892 (2015).
29. X. Niu, X. Hu, S. Chu, and Q. Gong, "Epsilon-near-zero photonics: A new platform for integrated devices," Adv. Opt. Mater. **6**(10), 1701292 (2018).
30. R. Maas, J. Parsons, N. Engheta, and A. Polman, "Experimental realization of an epsilon-near-zero metamaterial at visible wavelengths," Nat. Photonics **7**(11), 907–912 (2013).
31. L. V. Alekseyev, E. E. Narimanov, T. Tumkur, H. Li, Y. A. Barnakov, and M. A. Noginov, "Uniaxial epsilon-near-zero metamaterial for angular filtering and polarization control," Appl. Phys. Lett. **97**(13), 131107 (2010).
32. G. Subramania, A. J. Fischer, and T. S. Luk, "Optical properties of metal-dielectric based epsilon near zero metamaterials," Appl. Phys. Lett. **101**(24), 241107 (2012).
33. J. Gao, L. Sun, H. Deng, C. J. Mathai, S. Gangopadhyay, and X. Yang, "Experimental realization of epsilon-near-zero metamaterial slabs with metal-dielectric multilayers," Appl. Phys. Lett. **103**(5), 051111 (2013).
34. S. I. Maslovski and M. G. Silveirinha, "Nonlocal permittivity from a quasistatic model for a class of wire media," Phys. Rev. B Condens. Matter Mater. Phys. **80**(24), 245101 (2009).
35. C. Della Giovampaola and N. Engheta, "Plasmonics without negative dielectrics," Phys. Rev. B **93**(19), 195152 (2016).
36. Z. Li, L. Liu, H. Sun, Y. Sun, C. Gu, X. Chen, Y. Liu, and Y. Luo, "Effective surface plasmon polaritons induced by modal dispersion in a waveguide," Phys. Rev. Appl. **7**(4), 044028 (2017).
37. F. R. Prudêncio, J. R. Costa, C. A. Fernandes, N. Engheta, and M. G. Silveirinha, "Experimental verification of 'waveguide' plasmonics," New J. Phys. **19**(12), 123017 (2017).
38. Z. Li, Y. Sun, K. Wang, J. Song, J. Shi, C. Gu, L. Liu, and Y. Luo, "Tuning the dispersion of effective surface plasmon polaritons with multilayer systems," Opt. Express **26**(4), 4686–4697 (2018).
39. Y. Li and Z. Zhang, "Experimental verification of guided-wave lumped circuits using waveguide metamaterials," Phys. Rev. Appl. **9**(4), 044024 (2018).
40. Y. Li, I. Liberal, C. Della Giovampaola, and N. Engheta, "Waveguide metatronics: Lumped circuitry based on structural dispersion," Sci. Adv. **2**(6), e1501790 (2016).
41. W. Cai and V. Shalaev, *Optical metamaterials: Fundamentals and applications* (Springer, 2009).
42. W. Śmigaj and B. Gralak, "Validity of the effective-medium approximation of photonic crystals," Phys. Rev. B Condens. Matter Mater. Phys. **77**(23), 235445 (2008).
43. J. Luo, Y. Yang, Z. Yao, W. Lu, B. Hou, Z. H. Hang, C. T. Chan, and Y. Lai, "Ultratransparent media and transformation optics with shifted spatial dispersions," Phys. Rev. Lett. **117**(22), 223901 (2016).
44. F. E. Gardiol, "Anisotropic slabs in rectangular waveguides," IEEE T. Microw. Theory **18**(8), 461–467 (1970).
45. Y. Xu, "A study of waveguides filled with anisotropic metamaterials," Microw. Opt. Technol. Lett. **41**(5), 426–431 (2004).
46. V. A. Podolskiy, and E. E. Narimanov, "Strongly anisotropic waveguide as a nonmagnetic left-handed system," Phys. Rev. B **71**, 201101 (2005).
47. X. Huang, Y. Lai, Z. H. Hang, H. Zheng, and C. T. Chan, "Dirac cones induced by accidental degeneracy in photonic crystals and zero-refractive-index materials," Nat. Mater. **10**(8), 582–586 (2011).

Optics EXPRESS

48. C. Xu, G. Wang, Z. H. Hang, J. Luo, C. T. Chan, and Y. Lai, "Design of full-k-space flat bands in photonic crystals beyond the tight-binding picture," Sci. Rep. **5**(1), 18181 (2015).
49. J. Luo, Y. Lai, and C. T. Chan, "Control of electromagnetic flux in inhomogeneous anisotropic media," in *Transformation Wave Physics - Electromagnetics, Elastodynamics, and Thermodynamics*, M. Farhat, P. Chen, S. Guenneau and S. Enoch, ed. (Pan Stanford Publishing, 2016).